Combining Protein-Shelled Platinum Nanoparticles with Graphene to Build a Bionanohybrid Capacitor

Boi Hoa San,[†,‡,#] Jang Ah Kim,[†,#] Atul Kulkarni,[§,∥] Sang Hyun Moh,[†,‡,∥] Sreekantha Reddy Dugasani,[⊥] Vinod Kumar Subramani,[‡] Nanasaheb D. Thorat,[‡] Hyun Ho Lee,[#] Sung Ha Park,[⊥] Taesung Kim,[*,†,§] and Kyeong Kyu Kim[*,†,‡]

[†]Sungkyunkwan Advanced Institute of Nanotechnology, Sungkyunkwan University, Suwon 440-746, Republic of Korea, [‡]Department of Molecular Cell Biology, Samsung Biomedical Research Institute, Sungkyunkwan University School of Medicine, Suwon 440-746, Republic of Korea, [§]School of Mechanical Engineering, Sungkyunkwan University, Suwon 440-746, Republic of Korea, [∥]BIO-FD&C & Co., Smart Valley A-510, Songdomirae-ro 30, Yeongsu-gu, Incheon, Republic of Korea, [⊥]Department of Physics, Sungkyunkwan University, Suwon 440-746, Republic of Korea, and [#]Department of Chemical Engineering, Myongji University, Yongin 449-728, Republic of Korea. [#]B. H. San and J. A. Kim contributed equally to this work.

ABSTRACT The electronic properties of biomolecules and their hybrids with inorganic materials can be utilized for the fabrication of nanoelectronic devices. Here, we report the charge transport behavior of protein-shelled inorganic nanoparticles combined with graphene and demonstrate their possible application as a bionanohybrid capacitor. The conductivity of PepA, a bacterial aminopeptidase used as a protein shell (PS), and the platinum nanoparticles (PtNPs) encapsulated by PepA was measured using a field effect transistor (FET) and a graphene-based FET (GFET). Furthermore, we confirmed that the electronic properties of PepA-PtNPs were controlled by varying the size of the PtNPs. The use of two poly(methyl methacrylate) (PMMA)-coated graphene layers separated by PepA-PtNPs enabled us to build a bionanohybrid capacitor with tunable properties. The combination of bioinorganic nanohybrids with graphene is regarded as the cornerstone for developing flexible and biocompatible bionanoelectronic devices that can be integrated into bioelectric circuits for biomedical purposes.

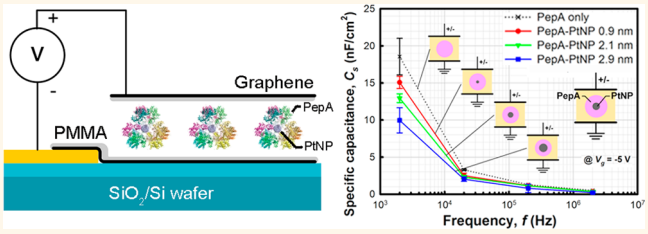

KEYWORDS: protein shell · pepA · platinum nanoparticle · graphene · capacitor · bionanohybrid

The combination of biological materials and inorganic materials can yield multifunctional hybrid materials with new functional properties. Among these hybrids, protein-shelled nanoparticles (PSNPs),[1−5] inorganic nanoparticles encapsulated by oligomeric proteins with a hollow center, are highly potent and have various applications including biomedicines,[6−9] biocatalysts,[10,11] and bioelectronic devices.[12] In this type of integration, protein shells (PSs) are used as biotemplates for the synthesis of a variety of inorganic nanoparticles including metals,[4,5] semiconductors,[13,14] and magnets.[8,15] The advantages of using PSs include not only protecting the various nanoparticles (NPs) with precise size control but also increasing the stability of NPs and reducing their toxicity. For these reasons, PSNPs are considered good candidates for biomedical applications such as nanobiosensors. However, since protein itself has poor electric properties, its applications to bioelectronic devices are relatively limited even after it is combined with metallic materials.

To date, there have been only a few reports on the application of PSNPs to the fabrication of electronic devices, and this is mainly due to the lack of information regarding the charge transport properties of PSNPs. For the fabrication of floating nanodot gate memory (FNGM) devices, $5Fe_2O_3 \cdot 9H_2O$ (ferrihydrite) and Co_3O_4 NPs encapsulated by apoferritin were used to construct an array of charge storage nodes, and the I_D-V_G characteristic curves of the fabricated FNGM were constructed.[12,16] However, in those cases, since the PSs were eliminated by heat treatment before the electronic properties of the inorganic NPs were measured, the contribution of the PSs

* Address correspondence to kyeongkyu@skku.edu, tkim@skku.edu.

Received for review June 11, 2014 and accepted November 26, 2014.

Published online November 26, 2014
10.1021/nn503178t

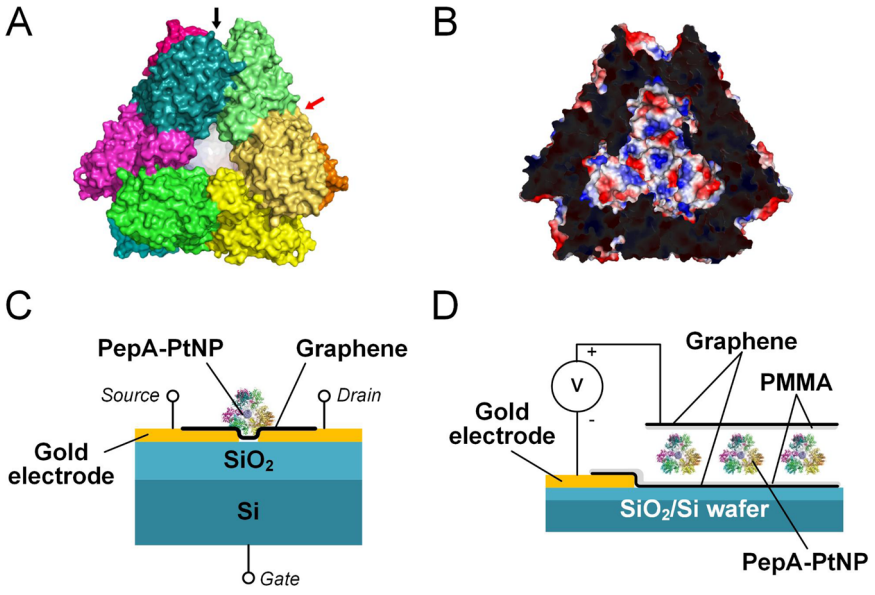

Figure 1. Overall structure of PepA (PDB ID: 3KL9). (A) Surface presentation of a dodecameric PepA. Each subunit is presented in different colors. Black and red arrows indicate small and large channels, respectively, located at the interface of each subunit. (B) Interior surface of PepA is presented with surface charge distribution in the same orientation as part A. Red and blue colors on the surface represent negative and positive charges, respectively. The internal and external diameters of PepA are 6.0 and 12 nm, respectively. (C) Schematic diagram of the GFET device with PepA-PtNP. PepA-PtNPs were loaded on a graphene layer connected to drain and source electrodes. Source, drain, and gate are indicated. The distance between the source and drain is 5 μm. (D) Schematic diagram of PepA-PtNPs biocapacitor. PepA-PtNPs were loaded in between graphene capacitor electrodes insulated with PMMA layers. The area of the biocapacitor was 0.25 cm^2.

to the charge transfer characteristics was not investigated. For biomedical applications of PSNPs and the construction of bioelectronic devices, it is still necessary to elucidate the electronic properties of bionanohybrid materials.

Carbon-based nanomaterials such as carbon nanotubes (CNTs) and graphene have been intensively studied due to their nanoscopic and unique electrical properties. For instance, CNTs used in constructing field effect transistor (FET) devices[17] were developed as sensors for the detection of various biomolecules.[18] However, recent studies have proven that graphene, with its two-dimensional honeycomb structure that is only one atom thick, has greater potential than CNTs for applications in electrical devices and biosensors since it has many advantages in electronic fabrication such as higher electrical conductivity, physical flexibility, biocompatibility, and large surface area.[19−24] In particular, it was proven that the graphene-based FET biosensors detect biomolecules with higher sensitivity.[25] As a result, we expected that the combination of bioinorganic nanohybrid materials such as PSNPs and a graphene-based device could result in functional materials with novel properties that can be integrated into biodevices or circuits for biomedical purposes such as implanted biosensors.

PepA, a dodecameric bacterial aminopeptidase from *Streptococcus pneumonia*, has been used as a PS for PSNP construction.[26] PepA assembles into a hollow tetrahedral shape with 6 and 12 nm interior and exterior diameters, respectively, and with four 3.0 nm diameter channels and four 1.0 nm diameter channels at the interfaces between each pair of subunits (Figure 1A and B).[27] The advantage of using PepA for the synthesis of NPs is the precise control of the size of NPs inside the PepA, ranging from 0.9 to 3.2 nm, by varying the conditions for NP synthesis.[5] The application of PepA-NPs in various fields has been demonstrated, including use of PepA-PtNPs as a multifunctional nanobiocatalyst[5] and biocompatible ROS (reactive oxygen species) quencher[26] and the use of PepA-CoPt as a MRI contrasting agent.[28] PtNPs are considered to be more advantageous for constructing electronic devices than other semiconductors or metal NP-based capacitors.[16,29] It is due to the high work function (5.65 eV) and chemical stability, which are necessary for enhancing the retention characteristics without forfeiting injection efficiency.[29,30] Therefore, it is expected that PepA-PtNPs can be possibly applied for fabricating a new bioelectronic device. In addition, their integration with graphene will provide a new opportunity to build a novel bionanocapacitor, since the dielectric PS combines PtNP and graphene.

To investigate the possible application of PepA-PtNPs in combination with graphene to electronic fabrication, we examined the charge transport behaviors of PepA-PtNPs with and without graphene by fabricating FET devices in an ambient atmosphere at room temperature (RT) in the solution phase. Then, frequency-modulated capacitor devices were assembled by sandwiching PepA-PtNPs with graphene layers, and their electrical conductivity was further

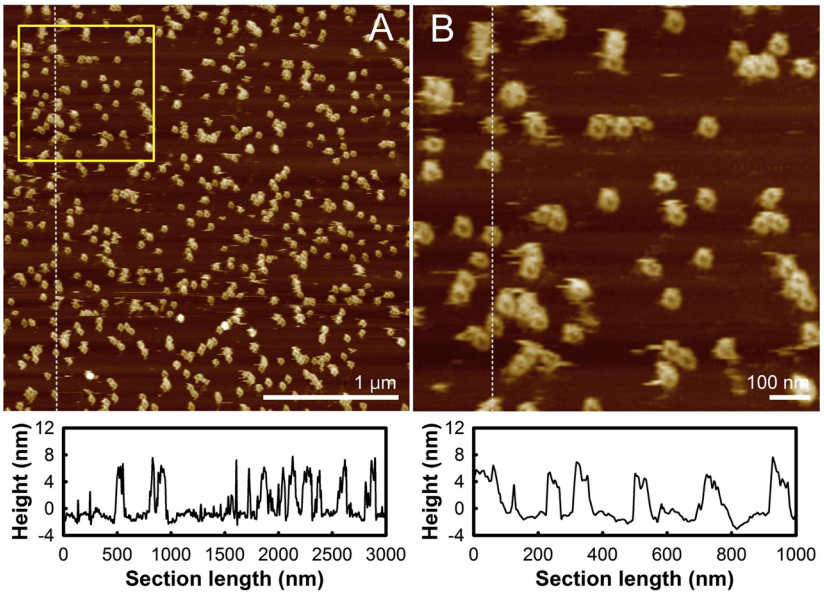

Figure 2. Liquid phase AFM images for the surface morphology of PepA-PtNP deposited on mica surface (A). (B) AFM image representing a magnified image of the corresponding box in A. The scale bars are 1000 and 100 nm for A and B, respectively. The height profiles along the dotted lines in A and B are also displayed.

analyzed. These devices showed tremendously enhanced charge trap and charge transport behaviors, proving that PepA-PtNPs are suitable for the fabrication of bionanoelectronic devices, which will be the first step in building bionanoelectronic circuits.

RESULTS AND DISCUSSION

PtNPs, synthesized and stabilized using bacterial peptidase PepA, were mostly spherical and monodisperse without aggregation (see Supporting Figure S1). The synthesis efficiency was estimated to be 100% based on an examination of 250 individual PepA-PtNPs in electron microscopy images, indicating that they are suitable for building electronic devices with high homogeneity. By manipulating the initial molar ratio between the precursor Pt ions and PepA, 0.9, 2.1, and 2.9 nm PtNPs encapsulated by PepA were synthesized with narrow size distributions (see Supporting Figure S1). To characterize the electronic properties of the PepA-PtNPs, 2.1 nm PepA-PtNPs were used in the current study unless otherwise stated.

Atomic force microscopy (AFM) was employed to analyze the morphology of PepA-PtNPs deposited on substrates (Figure 2 and see Supporting Figure S2) and verified that proteins are evenly and individually dispersed. The average height and diameter of PepA-PtNPs on a flat surface were 8 and 22 nm, respectively (Figure 2), which are close to the overall dimensions of PepA measured by crystallographic and TEM analyses[5,27] considering that the size of proteins cannot be precisely determined due to the squeezing effect in AFM measurements. In the case of AFM measurement of ferritin, a 24-subunit PS with a diameter of 12 nm, a heights as low as 4 nm, and diameters up to 30 nm was reported.[31] The AFM images of PepA-PtNPs deposited on the graphene surface at two different concentrations also revealed that they are well dispersed as a monolayer with similar height profile, although some protein aggregates or graphene wrinkles were observed on the surface (see Supporting Figure S2C−F). When the concentration of PepA-PtNPs deposited on the graphene surface varied from 0.1 to 0.5 μM, the surface coverage of PepA-PtNP on the graphene surface increased proportionally (see Supporting Figure S2 and Supporting Table S1). The AFM image of graphene without protein loading revealed that the graphene surface is flat with some wrinkles and roughness 1.0 nm thick (see Supporting Figure S2A,B).

A FET device was fabricated using a SiO_2/Si substrate containing gold microgap electrodes, which acted as a source and a drain (Figure 1C; see Supporting Figure S3). Detailed procedures for the device fabrication are provided in the Methods section. An aqueous solution containing PepA or PepA-PtNPs in various concentrations was harbored within the electrode gap, and the electron transport behaviors were subsequently analyzed (Figure 3A and B). The concentration dependence of the PepA-PtNPs conductivity was analyzed by monitoring the drain-to-source current (I_{ds}) as the drain-to-source voltage (V_{ds}) varied from −4 V to +4 V at a zero gate voltage (Figure 3A). The concentration dependency of I_{ds} was clearly revealed in the range of 0.0 to 1.0 V_{ds} (Figure 3A inset). When the concentration of PepA-PtNPs increased from 0.1 μM to 1.0 μM, conductivity increased from 16.8 μS/m to 26.3 μS/m. Thus, the conductivity of the PepA-PtNP-loaded FET was proportional to the concentration of PepA-PtNPs.

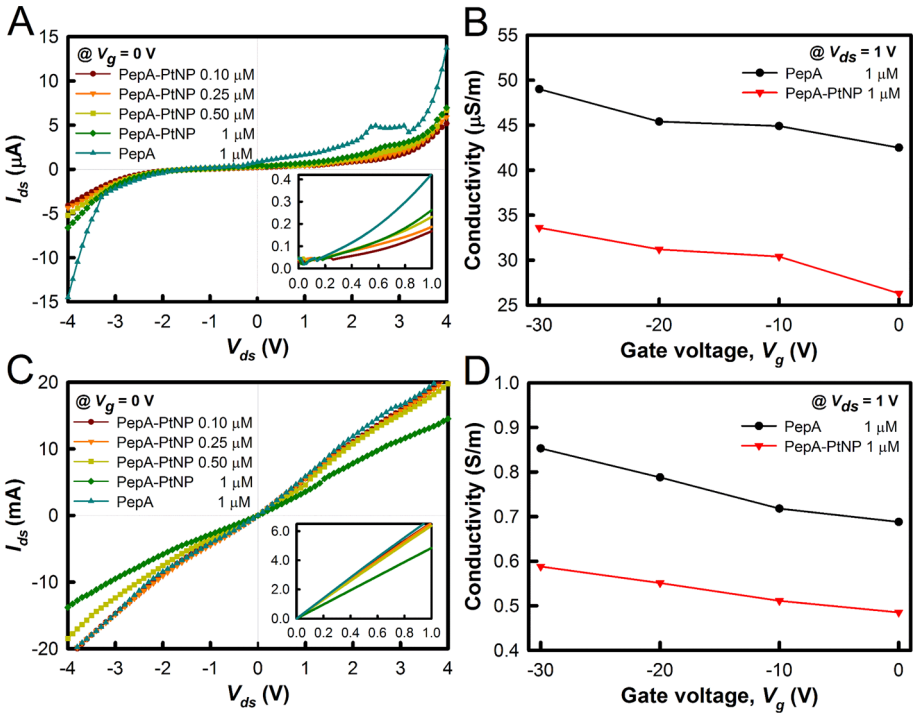

Figure 3. Electron transport behavior of PepA and PepA-PtNP in the FET and GFET devices. (A) $I_{ds}-V_{ds}$ characteristic curves of PepA-PtNP at various concentrations and PepA in FET at zero V_g. The abrupt increase in the current in the high-voltage region was caused by the increase in free electrons. The current (I_{ds}) change in response to V_{ds} in the voltage range from 0.0 to 1.0 V is shown in the inset. (B) Conductivity responses of 1 μM PepA and 1 μM PepA-PtNP in FET as a function of gate voltage (V_g). (C) $I_{ds}-V_{ds}$ characteristic curves of PepA-PtNP at various concentrations and PepA in GFET at zero V_g. The current (I_{ds}) change in response to V_{ds} is shown in the inset to display the linearity between I_{ds} and V_{ds} in the voltage range from 0.0 to 1.0 V. (D) Conductivity responses of 1-μM PepA and 1-μM PepA-PtNP in GFET as a function of V_g. The concentrations of PepA and PepA-PtNP refer to the protein concentration.

The mechanism of charge transport in biological molecules such as proteins and DNA has been intensively investigated, but is still controversial.[32−35] It has been proposed that electrical conduction through the protein is caused by electron transfer through direct quantum tunneling (superexchange) or sequential hopping.[32−35] In the same way, the electric current through PepA or PepA-PtNPs can also be explained by the electron transfer between adjacent PepA molecules in the aqueous solution. The detailed mechanism needs to be evaluated by further studies. Interestingly, at a given concentration, it was observed that the drain-to-source current of PepA-PtNPs was lower than that of PepA alone (Figure 3A), suggesting that the charge transport through PepA is likely to be trapped and hindered by PtNPs mineralized within PepA. It has been reported that smaller PtNPs can act as electron acceptors due to the lower density of d-electrons near the Fermi level than those of the large PtNPs or bulk Pt.[36] This interpretation might justify the lower charge transport in PepA-PtNPs. As it is, electrical conduction decreased due to the charge trapping by PtNPs. From this perspective, both the charge transport and trapping must be considered to understand the detailed mechanism underlying the electronic transport in PepA-PtNPs.

Further evaluations were conducted by applying back gate voltages (V_g) from −30 to 0 V (Figure 3B). As in the earlier discussion, PepA showed higher conductivity than PepA-PtNPs, and the conductivity difference was about 16 μS/m through the whole gate voltage range (Figure 3B). Interestingly, when the 2.4 nm PtNPs stabilized by citrate[37] were mixed with PepA instead of being encapsulated by PepA, their conductance was similar to that of the PtNPs and about 3-fold higher than that of the PtNPs encapsulated by PepA (Figure 3B and see Supporting Figure S4A). These data strongly suggest that the metallic properties of PtNPs are significantly modified when the particles are encapsulated in a PepA shell.

We further investigated the charge transport properties of PepA-PtNPs using a graphene-based FET (GFET). A graphene monolayer prepared by chemical vapor deposition (CVD; see Supporting Figure S5) was transferred onto a FET device for the fabrication of the GFET (Figure 1C). Measurements of the charge transport properties of PepA and PepA-PtNPs were carried out in the GFET device in a manner similar to that used with the FET device (Figure 3C and D; see Supporting Figure S6). The most interesting feature of the charge transport properties in GFET compared to that in FET is the presence of an ohmic junction, which is represented by a straight $I-V$ curve passing through the origin in the $I_{ds}-V_{ds}$ graph (Figure 3C). The ohmic junction is considered to be achieved by improved

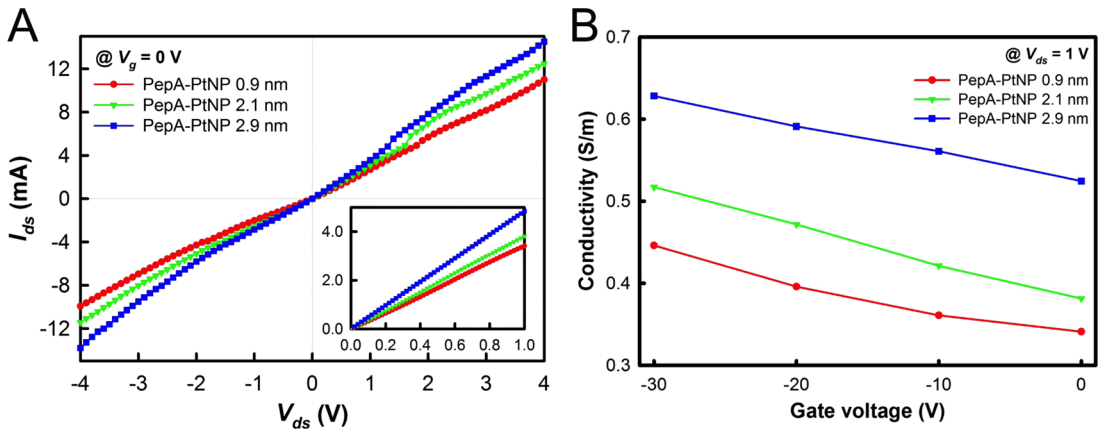

Figure 4. Electron transport behavior of different size PepA-PtNPs. (A) *I*−*V* characteristics of the PepA-PtNP in the GFET device with 0.9, 2.1, and 2.9 nm PtNPs at zero gate voltage. The conductance of the PepA-PtNPs was directly proportional to the size of the PtNPs encapsulated in the PepA. The current response to the voltage is shown in the inset to display the linearity between current and voltage in the voltage range from 0.0 to 1.0 V. (B) Conductivity responses of different size PepA-PtNPs in GFET as a function of a V_g.

contact between the gold electrode and graphene (Figure 1C; see Supporting Figure S6).

Since graphene presents P-type conducting behavior[38] by exhibiting a drain current change in response to the negative gate bias, the conductivity of the PepA-PtNPs on the GFET was measured by applying a negative gate voltage (see Supporting Figure S6). While the conductivities of PepA and PepA-PtNPs in the FET device were on the μS/m scale, those in the GFET device were on the sub-mS/m scale. For example, the conductivities of PepA-PtNPs were 26.3 μS/m and 0.49 S/m in the FET and GFET devices, respectively, at zero gate voltage (V_g) (Figure 3B and D), indicating that the conductivity in the GFET device was about 4 orders of magnitude higher than that in the FET device. The enhanced conductance of the PepA/GFET was expected, since it was reported that protein adsorption to graphene enhances the conductance of GFET.[39]

Similar to the observation in the FET devices, the conductivity of PepA-PtNPs was lower than that of PepA in the GFET device (Figure 3C); specifically, the conductivities were 0.49 S/m for PepA-PtNPs and 0.69 S/m for PepA at a 1.0 μM concentration. The reduced conductance of the PepA-PtNP/GFET is likely to be caused by charge trapping from graphene to the PtNPs through the PSs, which is similar to the case of the FET device (Figure 3A). The calculated electron mobility of PepA (1.0 μM) and PepA-PtNP (1.0 μM) was 3190 and 2002 cm^2/V.s, respectively. These data also support that the decrease in conductivity is due to the electron trapping of PtNPs. However, the conductivity of PtNPs alone is similar to that of PtNPs mixed with PepA in GFET, demonstrating that PepA alone did not have any significant effect on the PtNPs when it is simply mixed (see Supporting Figure S4B).

Interestingly, while I_{ds} and the concentration of PepA-PtNPs were directly correlated when they were integrated in the FET device (Figure 3A), they were inversely correlated in the GFET device. That is, the conductivity of PepA-PtNPs in the GFET device decreased from 0.66 S/m to 0.49 S/m when the concentration of PepA-PtNPs was increased from 0.1 μM to 1.0 μM (Figure 3C). These results suggest that the charge-trapping effect of PtNPs is more significant in GFET than in FET. It is noticeable that the surface coverage of PepA-PtNP increases in proportion to the concentration of PepA-PtNP (see Supporting Table S1). The enhanced charge trapping effect of PtNPs in GFET than in FET may be explained by the effect of physical adsorption of PepA-PtNPs on the graphene surface. Electrons may flow from graphene into PtNPs due to the difference of the work function: 4.5 eV for graphene[40,41] *vs* 5.65 eV for PtNP.[30] Therefore, the charge redistribution at the interface between graphene and PepA-PtNPs can possibly cause the drain current decrement in the GFET device response.[40] Therefore, both the positive effect of PepA and graphene and the negative effect of PtNPs on electron transport should be considered simultaneously in order to understand the concentration dependency of the PepA-PtNP conductivity in the FET and GFET devices.

In order to investigate the size effect of the PtNPs on the charge transfer activity of the PepA-PtNPs in the GFET device, we synthesized PepA-PtNPs with sizes of 0.9, 2.1, and 2.9 nm (see Supporting Figure S1). For each measurement, the same number of PtNPs encapsulated by PepA was used in order to monitor only the effect of the size on the transport property by applying the same concentration of PepA. The drain current or conductivity was directly proportional to the size of the PtNPs, and the differences were maximized at high V_{ds} (Figure 4). It is known that the work function of metal NPs is inversely proportional to the size of the NPs.[42,43] Hence, the charge trapping capability of smaller PtNPs is expected to be higher than that of bigger PtNPs.[36]

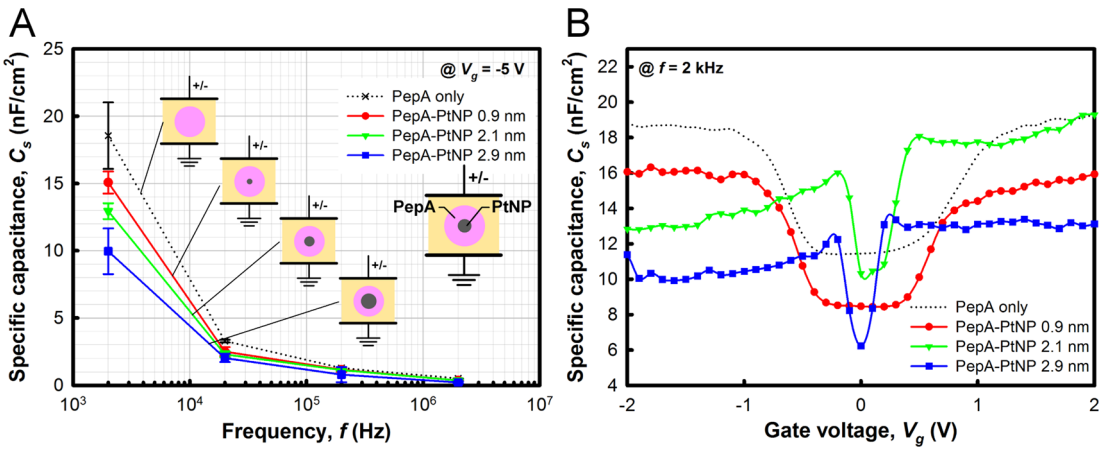

Figure 5. (A) Capacitance−frequency ($C-f$) curves of the PepA and PepA-PtNPs bionanohybrid capacitor display specific capacitances that vary according to the applied perturbing frequencies for various sizes of PepA-PtNP capacitors at −5 V gate voltage. High capacitance was observed at low frequency, and the capacitance decreased as the size of the PtNP increased possibly due to the polarizability effects. The insets indicate the structure of the bionanohybrid capacitor with different sizes of PtNP encapsulated inside PepA. The capacitance of the PepA-PtNPs bionanohybrid capacitor was measured using a semiconductor characterization system (SCS) in the strong accumulation region, which is the range in which the voltage-independent insulator capacitance appears. (B) Capacitance−voltage ($C-V$) curves of the PepA-PtNPs bionanohybrid capacitor. Specific capacitance measured as a function of gate voltage (V_g, −2.0 to 2.0 V) at low frequency, 2 kHz, showed a highly symmetric profile.

Consequently, the 2.9 nm PepA-PtNPs showed the maximum conductivity, possibly due to the lower trapping activity of PtNPs (Figure 4). These results strongly suggest that the electronic transport properties can be precisely manipulated by controlling the size of the PtNPs. Therefore, it is advantageous to use PepA-PtNPs rather than to use PepA alone for the fabrication of electronic devices.

The current investigation reveals that the electron transport properties of PepA-PtNPs can be measured using FET and GFET devices. In addition, it was also observed that their electronic properties can be manipulated by PepA-PtNPs as a function of the concentration and the size of the NPs. From these observations, we hypothesized that PtNPs encapsulated by PSs combined with graphene can be used for fabricating a bionanohybrid capacitor, in which the PepA-PtNPs can trap electrons and enhance the capacitance.

To examine this hypothesis, we fabricated a symmetric multilayered bionanocapacitor by putting PepA-PtNPs of various sizes between the bottom and upper graphene layers coated with poly(methyl methacrylate) (PMMA) (Figure 1D). This forms a structure similar to the metal−insulator−semiconductor−insulator−metal (MISIM). The gate voltage (V_g) and ac voltages were applied to the graphene layers *via* a gold electrode and silver paste for the bottom and upper layers, respectively.

Then, the capacitance between the two electrodes contacting the graphene layers was measured as a function of frequency ($C-f$) for $V_g = -5.0$ V, which is within the strong accumulation region of the measured capacitance (Figure 5). The $C-f$ curves of the fabricated bionanocapacitor showed a clear trend of decreasing specific capacitance when the frequency increases from 2 kHz to 2000 kHz (Figure 5A). Ideally, the MISIM specific capacitance is constant for the change in frequency.[44] However, it is known that capacitance with charge polarization can vary in response to the frequency due to the change in relaxation time of charge polarization.[45] At higher frequency, the charging effect does not respond well to ac signals, and the polarizability of the capacitor decreases. Consequently, at higher frequency the capacitance decreased. Since the current bionanocapacitor has a lower capacitance in the higher frequency range and the specific capacitance was inversely proportional to the frequency (Figure 5A), the polarizability of PepA-PtNP seems to contribute to the capacitance. Most importantly, the current bionanocapacitors clearly showed a decreasing trend of capacitance with increasing sizes of PtNPs in both $C-f$ and $C-V$ graphs (Figure 5). Accordingly, the bionanocapacitor with PepA showed a higher capacitance than only those harboring the PtNPs inside (Figure 5). These results are possibly due to the fact that the polarizability of the PepA-PtNP layer is largely dependent upon the size of PtNPs encapsulated inside PepA (Figure 5).

For further characterization of the electronic properties of the current device, the gate voltage dependences of the PepA-PtNP and PepA-only bionanocapacitors were examined at a low frequency, 2 kHz, where the carriers follow the ac signal. Interestingly, they showed very distinctive $C-V$ characteristics (Figure 5B). In general, a MIS capacitor does not show symmetric switching responses, but does show asymmetric U-shaped and step-like responses for lower and higher frequency, respectively. In addition, the dynamic states of the capacitor (*i.e.*, accumulation, depletion, and inversion) can also be detected when various gate

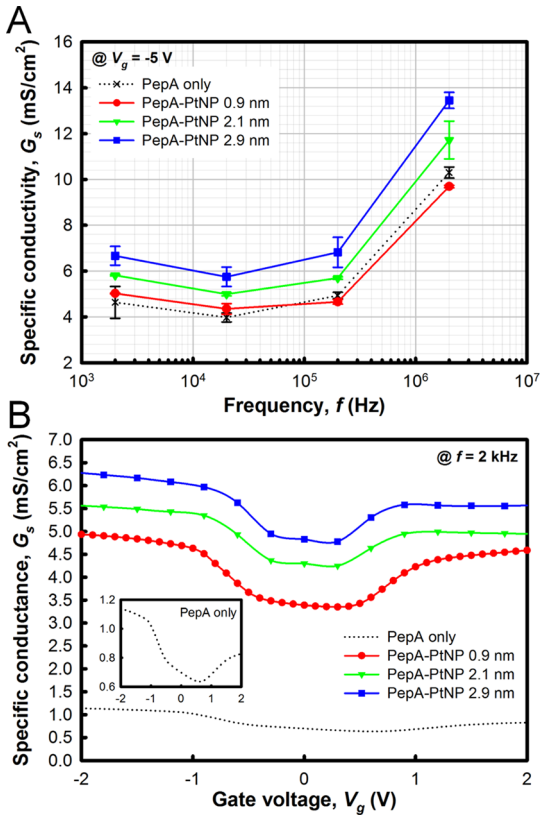

Figure 6. Conductance–frequency and conductance–voltage characteristics for the PepA and PepA-PtNPs bionanohybrid capacitor. (A) Frequency dependence of the specific conductance at a −5 V applied gate voltage is displayed in conductance–frequency (G–f) curves. (B) The change in the specific conductance of the PepA-PtNPs bionanohybrid capacitor as a function of gate voltage (V_g) is shown in conductance–voltage (G–V) curves. The conductance was measured at 2 kHz.

voltages were applied.[46] However, the PepA-PtNP bionanocapacitors showed a U-shaped symmetric response centered at zero gate voltage (V_g = 0 V) (Figure 5B).

Then, the conductance of the PepA-PtNP and PepA-only bionanocapacitors were investigated in terms of frequency and gate voltage dependence (Figure 6). For the frequency-dependent conductance (G–f) plot, a log–log scale is commonly adopted, as shown in Figure 6A. At the lower f range, the G value was insensitive to frequency, but it slightly increased at frequencies higher than 200 kHz (Figure 6A). Although the G–f relationships of disordered solids such as organic, amorphous, and doped semiconductors have been extensively studied,[47−54] those of biomolecular systems have not been intensively studied yet. To interpret the time-dependent behaviors of the PepA-PtNP bionanocapacitor, it is of interest to consider the tunneling and hopping mechanism of charge transport. For the biomolecules, the time required for electron tunneling is considered to be within the millisecond to microsecond range because their charge transport is originally based on the redox reaction.[55] Therefore, under the conditions of electron tunneling, it is expected that the specific conductance decreases with respect to the frequency increase in the kHz to MHz range. In contrast, time-dependent hopping conductivity is known to be insensitive to the varying f in the log–log scale.[56] Therefore, based on the G–f curve of the PepA-PtNP bionanocapacitor (Figure 6A), the time-dependent charge transport behavior of the bionanocapacitor can be partially explained by the hopping conduction mechanism. Under this situation, the increase in G in the higher f region is assumed to be caused by the delocalized electrons due to the higher vibrational energy. We further measured the conductance-applied voltage (G–V) responses of the device (Figure 6B). Similar to the C–V curves (Figure 5B), the conductance is high in the far-negative V_g region and minimum in the near-zero V_g region in the G–V curve. However, the width of the U-shape region in each G–V curve is broader than those of the C–V curves (Figure 6B *vs* Figure 5B). The conductance in PepA-PtNP bionanocapacitors was at least 5 times higher than that of PepA, and this increase was solely due to the integration of PtNPs inside PepA (Figure 6B). Taken together, it seems to be possible to choose a gate voltage where the bionanocapacitor shows a high capacitance but low conductance, which enables maximizing the bionanocapacitor's charge storage characteristics.

CONCLUSIONS

We have investigated the charge transport phenomena of PepA-PtNP, a bioinorganic nanohybrid material, using FET devices with and without graphene in an ambient atmosphere and at RT. The PtNPs affected the electronic properties of PepA and graphene by capturing electrons, and thus the electronic properties of PepA-PtNPs in the GFET were modulated by varying the size and concentration of the PtNPs encapsulated by the PepA. PepA-PtNP/GFET showed higher electron mobility than other well-known FET devices (see Supporting Table S2). On the basis of these findings, we have successfully fabricated a bionanohybrid MISIM capacitor by combining graphene and PepA-PtNPs and demonstrated that the bionanohybrid capacitor could operate in a stable manner with ambipolar characteristics. This novel bionanocapacitor displayed relatively enhanced charge trap and charge transport behaviors, compared with other biomolecule-based electronic devices (see Supporting Table S3), thus proving that PepA-PtNPs are suitable for further development of fast and efficient bionanoelectronic devices. Moreover, we also showed the capacitance can be controlled by varying the size of the PtNPs. Since it has already been proven that graphene has many useful characteristics such as high sensitivity, fast responsiveness, physical flexibility, and biocompatibility, it is expected that PepA-PtNP bionanohybrid capacitors

made with a graphene will have these useful characteristics. Thus, these capacitors should be suitable for various biotechnological applications such as biosensors or therapeutics embedded into a human body. Therefore, the current study opens the door for future fabrication of biodevices and biocircuits by demonstrating the possibility of developing bioinorganic materials as a capacitor.

METHODS

Sample Preparation. The preparation of PepA and the synthesis of the platinum nanoparticles (PtNPs) using PepA were described previously.[5,27] In brief, the *in situ* synthesis of the PtNPs was performed in solution by precipitating Pt^{2+} in PepA at RT. The purified recombinant PepA was mixed with K_2PtCl_4 in 10 mL of buffer A [50 mM HEPES, 4-(2-hydroxyethyl)-1-piperazineethanesulfonic acid, pH 8.0] at various molar ratios and was incubated for 1 h with constant stirring. For the synthesis of the 1:1000 PepA:PtNPs, 1 μM and 1 mM of PepA and K_2PtCl_4, respectively, were mixed in the reaction solution. After the addition of 0.5 mL of a 100 mM ice-cold $NaBH_4$ solution, the reaction mixture was incubated at RT for 5 h with stirring. The reaction mixture was concentrated using a Centricon with a 30 kDa cutoff (Sartorius, Gottingen, Germany) and was centrifuged at 16 100 rcf for 30 min at 4 °C. Finally, the sample was further purified using a Superdex 200 gel filtration column (GE Healthcare, Princeton, NJ, USA) in distilled water (DW). In this study, DW was prepared using a Millipore Milli-Q system with a resistivity of 18.2 MΩ·cm at 25 °C (EMD Millipore, Billerica, MA, USA). The final product in DW was used for the measurement of the current−voltage characteristics. The concentration of PepA was determined by the Bradford assay.[57]

Characterization of PepA-PtNPs and Graphene. PepA-PtNPs were characterized in a manner similar to that described in a previous report.[5] Transmission electron microscopy (TEM) images were obtained using JEOL JEM-3010 and JEOL JEM-2100 microscopes (JEOL, Tokyo, Japan) operated at 200 kV. TEM samples were prepared by applying the PepA-PtNP solution onto a copper grid covered with a thin carbon film (JEOL, Tokyo, Japan) for overnight dehydration at RT. For preparation of the negatively stained PepA-PtNP samples, the sample in the copper grid was stained with 2% uranyl acetate for 30 s. The sizes of the PtNPs were estimated by averaging 200 enlarged images that were measured using Gatan Digital Micrograph software (Gatan, Pleasanton, CA, USA).

The topology of the graphene surface and the thickness of the graphene layer were measured using an atomic force microscope (AFM) (Innova; Veeco, Plainview, NY, USA) on the 200 nm SiO_2/Si substrate. The AFM was operated in tapping mode at a frequency of 282.5 kHz using an aluminum-coated silicon cantilever (NanoWorld AG, Switzerland) with a pyramidal tip having a radius of 8 nm. For each graphene film, three independent areas with dimensions of 2 μm × 2 μm were analyzed by scanning them at a resolution of 512 × 512 scan lines. Raman spectra of the graphene monolayer on a 200 nm SiO_2/Si substrate were measured at 532 nm using a confocal Raman microscope (alpha-300R; WITec, Maryville, TN, USA) at RT.

Synthesis and Transfer of Graphene on a SiO_2 Substrate. The experimental procedure for the growth of the graphene layer was similar to that described in our previous reports[58,59] with a deposition temperature ranging from 950 to 1000 °C. The graphene layers were grown using the chemical vapor deposition (CVD) method with methane (CH_4) and hydrogen (H_2) gas in a vacuum system. In the first step of synthesis, a copper foil was inserted into an 8-in. tube and then heated to 1050 °C with a flow of H_2 at 10 sccm and a pressure of 180 mTorr. Then, the sample was annealed at 1050 °C for 60 min at the same flow rate and pressure. The copper foils were heat-treated to increase the grain size from a few micrometers to ∼100 μm; as reported previously,[59] copper foils with larger grain sizes yielded higher-quality graphene films. The CH_4 and H_2 gases were then flowed at 1.6 Torr with rates of 28 and 10 sccm, respectively, for 30 min. Finally, the sample was rapidly cooled to RT (∼10 °C/s) with a flow of H_2 at 10 sccm and a pressure of 180 mTorr.

AFM Analysis. For AFM imaging of PepA-PtNP on a graphene/200 nm SiO_2/Si layer, 10 μL of analytes was dropped on the graphene surface and 5 μL of deionized water was mounted onto the AFM tip [an NP-S oxide-sharpened silicon nitride tip (Veeco). AFM images were obtained using Multimode Nanoscope (Veeco) in fluid tapping mode.

Fabrication and *I*−*V* Measurements of PepA-PtNPs FET and GFET. The CVD-grown graphene samples were spin-coated with PMMA, with the spinning speed ranging from 300 to 4000 rpm, depending on the size of the sample. After the PMMA coating, the graphene layer on the Cu foil was placed in an aqueous solution containing 0.1 M ammonium persulfate to etch off the Cu substrate. Afterward, the PMMA-coated graphene was scooped out of the solution by the microgap FET device. The graphene-deposited microgap FET device was rinsed several times with DW after the PMMA was removed using acetone.

In the microgap FET device, seven source-and-drain electrodes with 5 μm gaps were loaded onto a 500 μm Si layer that served as a back gate. The electrode and Si layer were insulated by a 200 nm SiO_2 layer. The electrodes were composed of 5 nm titanium cores covered by 25 nm of gold. The *I*−*V* characteristics of the FET and GFET were investigated using a semiconductor characterization system (4200 SCS; Keithley Instruments, Inc., Cleveland, OH, USA). An aqueous solution containing PepA or PepA-PtNP of various concentrations was harbored within the electrode gap, and the electron transport behavior was subsequently analyzed. All measurements were recorded in the first three scans and averaged in order to avoid any protein damage possibly caused by the heat generated from repeated measurements. The *I*−*V* curve was measured by sweeping the drain-to-source voltage from −4 to +4 V at a zero gate voltage. The conductivity was calculated from the value of resistivity at a *1*−*V* drain voltage.

Calculation of the Electron Mobility. The electron motility was estimated using the following formula for the linear region of FET devices:

$$\mu = m_{\mathrm{lin}} \frac{L}{W} \frac{1}{V_{\mathrm{ds}}} \frac{1}{C_{\mathrm{ox}}}$$

where the m_{lin} is the slope of $I_{\mathrm{ds}}-V_{\mathrm{g}}$ at the fixed V_{ds}, L and W are the length and width of the channel, and C_{ox} is the capacitance of the SiO_2 layer. The measured m_{lin} of PepA only and PepA-PtNPs were 55.08 μA/V and 34.56 μA/V, respectively. The L and W are both 5 μm, and C_{ox} for the 200 nm thick SiO_2 layer is 172.65 μF/m^2.

Fabrication of a Capacitor and the Capacitance Measurement. For the measurement of capacitance, graphene was transferred onto a single gold electrode deposited 200 nm SiO_2/Si substrate 5 × 7 mm in size. The spin-coated PMMA layers were placed as the insulator in between the graphene layers. Next, 20 μL of 1 μM PepA-PtNPs in DW was deposited on the PMMA/graphene surface and was air-dried at RT for 24 h. The bottom PMMA/graphene electrode (on which the PepA-PtNPs had been deposited) was covered by another graphene/PMMA layer with silver paste contacts. In this setting, a symmetric sandwiched structure was formed, which can be interpreted as a metal−insulator−(semi)conductor−insulator−metal capacitor. The ac frequency and gate voltage dependent capacitance and conductance measurements were carried out using a semiconductor characterization system (4200 SCS; Keithley Instruments).

Conflict of Interest: The authors declare no competing financial interest.

Acknowledgment. This work was supported by a grant from the National Research Foundation of Korea (NRF-2013R1A1A2058893) to T.K. and a grant from the Next-Generation

BioGreen 21 Program (SSAC PJ008107) to K.K.K. B.H.S. thanks Dr. Nguyen Thanh Tien for valuable discussions.

Supporting Information Available: TEM images; AFM analysis; the conductivities of PtNP alone and PtNP mixed with PepA; characterization of the graphene film; electrical properties of graphene in the FET device; the changes of resistance with V_{ds} graph of graphene in the FET device; and supporting tables. This material is available free of charge *via* the Internet at http://pubs.acs.org.

REFERENCES AND NOTES

1. Meldrum, F. C.; Wade, V. J.; Nimmo, D. L.; Heywood, B. R.; Mann, S. Synthesis of Inorganic Nanophase Materials in Supramolecular Protein Cages. *Nature* **1991**, *349*, 684–687.
2. Douglas, T.; Young, M. Host-Guest Encapsulation of Materials by Assembled Virus Protein Cages. *Nature* **1998**, *393*, 152–155.
3. Flenniken, M. L.; Willits, D. A.; Brumfield, S.; Young, M. J.; Douglas, T. The Small Heat Shock Protein Cage from *Methanococcus jannaschii* Is a Versatile Nanoscale Platform for Genetic and Chemical Modification. *Nano Lett.* **2003**, *3*, 1573–1576.
4. Kang, S.; Lucon, J.; Varpness, Z. B.; Liepold, L.; Uchida, M.; Willits, D.; Young, M.; Douglas, T. Monitoring Biomimetic Platinum Nanocluster Formation Using Mass Spectrometry and Cluster-Dependent H_2 Production. *Angew. Chem., Int. Ed.* **2008**, *47*, 7845–7848.
5. San, B. H.; Kim, S.; Moh, S. H.; Lee, H.; Jung, D. Y.; Kim, K. K. Platinum Nanoparticles Encapsulated by Aminopeptidase: A Multifunctional Bioinorganic Nanohybrid Catalyst. *Angew. Chem., Int. Ed.* **2011**, *50*, 11924–11929.
6. Zhang, L.; Laug, L.; Munchgesang, W.; Pippel, E.; Gosele, U.; Brandsch, M.; Knez, M. Reducing Stress on Cells with Apoferritin-Encapsulated Platinum Nanoparticles. *Nano Lett.* **2010**, *10*, 219–223.
7. Wu, H.; Wang, J.; Wang, Z.; Fisher, D. R.; Lin, Y. Apoferritin-Templated Yttrium Phosphate Nanoparticle Conjugates for Radioimmunotherapy of Cancers. *J. Nanosci. Nanotechnol.* **2008**, *8*, 2316–2322.
8. Uchida, M.; Flenniken, M. L.; Allen, M.; Willits, D. A.; Crowley, B. E.; Brumfield, S.; Willis, A. F.; Jackiw, L.; Jutila, M.; Young, M. J.; *et al.* Targeting of Cancer Cells with Ferrimagnetic Ferritin Cage Nanoparticles. *J. Am. Chem. Soc.* **2006**, *128*, 16626–16633.
9. San, B. H.; Moh, S. H.; Kim, K. K. Investigation of the Heating Properties of Platinum Nanoparticles under a Radiofrequency Current. *Int. J. Hyperthermia* **2013**, *29*, 99–105.
10. Varpness, Z.; Peters, J. W.; Young, M.; Douglas, T. Biomimetic Synthesis of a H_2 Catalyst Using a Protein Cage Architecture. *Nano Lett.* **2005**, *5*, 2306–2309.
11. San, B. H.; Ha, E.-J.; Paik, H.-j.; Kim, K. K. Radiofrequency Treatment Enhances the Catalytic Function of an Immobilized Nanobiohybrid Catalyst. *Nanoscale* **2014**, *6*, 6009–6017.
12. Yamashita, I.; Iwahori, K.; Kumagai, S. Ferritin in the Field of Nanodevices. *Biochim. Biophys. Acta, Gen. Subj.* **2010**, *1800*, 846–857.
13. Iwahori, K.; Yoshizawa, K.; Muraoka, M.; Yamashita, I. Fabrication of ZnSe Nanoparticles in the Apoferritin Cavity by Designing a Slow Chemical Reaction System. *Inorg. Chem.* **2005**, *44*, 6393–400.
14. Xing, R. M.; Wang, X. Y.; Yan, L. L.; Zhang, C. L.; Yang, Z.; Wang, X. H.; Guo, Z. J. Fabrication of Water Soluble and Biocompatible CdSe Nanoparticles in Apoferritin with the Aid of EDTA. *Dalton Trans.* **2009**, 1710–1713.
15. Klem, M. T.; Willits, D.; Solis, D. J.; Belcher, A. M.; Young, M.; Douglas, T. Bio-Inspired Synthesis of Protein-Encapsulated CoPt Nanoparticles. *Adv. Funct. Mater.* **2005**, *15*, 1489–1494.
16. Moh, S. H.; San, B. H.; Kulkarni, A.; Kim, T.; Kim, K. K. Synthesis and Electric Characterization of Protein-Shelled Cdse Quantum Dots. *J. Mater. Chem. C* **2013**, *1*, 2412–2415.
17. Tans, S. J.; Verschueren, A. R. M.; Dekker, C. Room-Temperature Transistor Based on a Single Carbon Nanotube. *Nature* **1998**, *393*, 49–52.
18. Liang, F.; Chen, B. A Review on Biomedical Applications of Single-Walled Carbon Nanotubes. *Curr. Med. Chem.* **2010**, *17*, 10–24.
19. Schwierz, F. Graphene Transistors. *Nat. Nanotechnol.* **2010**, *5*, 487–96.
20. Maiti, U. N.; Lee, W. J.; Lee, J. M.; Oh, Y.; Kim, J. Y.; Kim, J. E.; Shim, J.; Han, T. H.; Kim, S. O. 25th Anniversary Article: Chemically Modified/Doped Carbon Nanotubes & Graphene for Optimized Nanostructures & Nanodevices. *Adv. Mater.* **2014**, *26*, 40–67.
21. Yun, J. M.; Kim, K. N.; Kim, J. Y.; Shin, D. O.; Lee, W. J.; Lee, S. H.; Lieberman, M.; Kim, S. O. DNA Origami Nanopatterning on Chemically Modified Graphene. *Angew. Chem., Int. Ed.* **2012**, *51*, 912–915.
22. Han, T. H.; Lee, W. J.; Lee, D. H.; Kim, J. E.; Choi, E.-Y.; Kim, S. O. Peptide/Graphene Hybrid Assembly into Core/Shell Nanowires. *Adv. Mater.* **2010**, *22*, 2060–2064.
23. Artiles, M. S.; Rout, C. S.; Fisher, T. S. Graphene-Based Hybrid Materials and Devices for Biosensing. *Adv. Drug Delivery Rev.* **2011**, *63*, 1352–1360.
24. Geim, A. K.; Novoselov, K. S. The Rise of Graphene. *Nat. Mater.* **2007**, *6*, 183–191.
25. Huang, X.; Yin, Z.; Wu, S.; Qi, X.; He, Q.; Zhang, Q.; Yan, Q.; Boey, F.; Zhang, H. Graphene-Based Materials: Synthesis, Characterization, Properties, and Applications. *Small* **2011**, *7*, 1876–1902.
26. San, B. H.; Moh, S. H.; Kim, K. K. The Effect of Protein Shells on the Antioxidant Activity of Protein-Encapsulated Platinum Nanoparticles. *J. Mater. Chem.* **2012**, *22*, 1774–1780.
27. Kim, D.; San, B. H.; Moh, S. H.; Park, H.; Kim, D. Y.; Lee, S.; Kim, K. K. Structural Basis for the Substrate Specificity of Pepa from *Streptococcus pneumoniae,* a Dodecameric Tetrahedral Protease. *Biochem. Biophys. Res. Commun.* **2010**, *391*, 431–436.
28. San, B. H.; Lee, S.; Moh, S. H.; Park, J.-G.; Lee, J. H.; Hwang, H.-Y.; Kim, K. K. Size-Controlled Synthesis and Characterization of CoPt Nanoparticles Using Protein Shells. *J. Mater. Chem. B* **2013**, *1*, 1453–1460.
29. Liu, Z.; Lee, C.; Narayanan, V.; Pei, G.; Kan, E. C. Metal Nanocrystal Memories-Part II: Electrical Characteristics. *IEEE Trans. Electron Devices* **2002**, *49*, 1614–1622.
30. Park, B.; Cho, K.; Koo, Y.-S.; Kim, S. Memory Characteristics of Platinum Nanoparticle-Embedded MOS Capacitors. *Curr. Appl. Phys.* **2009**, *9*, 1334–1337.
31. Yoshinobu, T.; Suzuki, J.; Kurooka, H.; Moon, W. C.; Iwasaki, H. AFM Fabrication of Oxide Patterns and Immobilization of Biomolecules on Si Surface. *Electrochim. Acta* **2003**, *48*, 3131–3135.
32. Waleed Shinwari, M.; Jamal Deen, M.; Starikov, E. B.; Cuniberti, G. Electrical Conductance in Biological Molecules. *Adv. Funct. Mater.* **2010**, *20*, 1865–1883.
33. Ron, I.; Sepunaru, L.; Itzhakov, S.; Belenkova, T.; Friedman, N.; Pecht, I.; Sheves, M.; Cahen, D. Proteins as Electronic Materials: Electron Transport through Solid-State Protein Monolayer Junctions. *J. Am. Chem. Soc.* **2010**, *132*, 4131–4140.
34. Jortner, J.; Bixon, M.; Langenbacher, T.; Michel-Beyerle, M. E. Charge Transfer and Transport in DNA. *Proc. Natl. Acad. Sci. U.S.A.* **1998**, *95*, 12759–12765.
35. Giese, B.; Amaudrut, J.; Kohler, A. K.; Spormann, M.; Wessely, S. Direct Observation of Hole Transfer through DNA by Hopping between Adenine Bases and by Tunnelling. *Nature* **2001**, *412*, 318–320.
36. Qiu, L. M.; Liu, F.; Zhao, L. Z.; Yang, W. S.; Yao, J. N. Evidence of a Unique Electron Donor-Acceptor Property for Platinum Nanoparticles as Studied by XPS. *Langmuir* **2006**, *22*, 4480–4482.
37. Turkevich, J.; Miner, R. S., Jr.; Babenkova, L. Further Studies on the Synthesis of Finely Divided Platinum. *J. Phys. Chem.* **1986**, *90*, 4765–4767.
38. Kim, S. N.; Kuang, Z.; Slocik, J. M.; Jones, S. E.; Cui, Y.; Farmer, B. L.; McAlpine, M. C.; Naik, R. R. Preferential Binding of

Peptides to Graphene Edges and Planes. *J. Am. Chem. Soc.* **2011**, *133*, 14480–14483.
39. Ohno, Y.; Maehashi, K.; Yamashiro, Y.; Matsumoto, K. Electrolyte-Gated Graphene Field-Effect Transistors for Detecting pH and Protein Adsorption. *Nano Lett.* **2009**, *9*, 3318–3322.
40. Giovannetti, G.; Khomyakov, P. A.; Brocks, G.; Karpan, V. M.; van den Brink, J.; Kelly, P. J. Doping Graphene with Metal Contacts. *Phys. Rev. Lett.* **2008**, *101*, 026803.
41. Khomyakov, P. A.; Giovannetti, G.; Rusu, P. C.; Brocks, G.; van den Brink, J.; Kelly, P. J. First-Principles Study of the Interaction and Charge Transfer between Graphene and Metals. *Phys. Rev. B* **2009**, *79*, 195425.
42. Schmidt-Ott, A.; Schurtenberger, P.; Siegmann, H. C. Enormous Yield of Photoelectrons from Small Particles. *Phys. Rev. Lett.* **1980**, *45*, 1284–1287.
43. Wood, D. M. Classical Size Dependence of the Work Function of Small Metallic Spheres. *Phys. Rev. Lett.* **1981**, *46*, 749–749.
44. Nicollian, E. H.; Brews, J. R. *MOS (Metal Oxide Semiconductor) Physics and Technology*; Wiley: New York, 1982.
45. Konofaos, N.; McClean, I. P.; Thomas, C. B. Characterisation of the Interface States between Amorphous Diamond-Like Carbon Films and (100) Silicon. *Phys. Status Solidi A* **1997**, *161*, 111–123.
46. Galup-Montoro, C.; Schneider, M. C. *The MOS Capacitor, MOSFET Modeling for Circuit Analysis and Design*; World Scientific: Singapore, 2007.
47. Elliott, S. R. A Theory of A.C. Conduction in Chalcogenide Glasses. *Philos. Mag.* **1977**, *36*, 1291–1304.
48. Dyre, J. C. The Random Free-Energy Barrier Model for AC Conduction in Disordered Solids. *J. Appl. Phys.* **1988**, *64*, 2456–2468.
49. Awan, S. A.; Gould, R. D. Conductivity and Dielectric Properties of Silicon Nitride Thin Films Prepared by RF Magnetron Sputtering Using Nitrogen Gas. *Thin Solid Films* **2003**, *423*, 267–272.
50. Gould, R. D.; Awan, S. A. Dielectric Properties of AlNx Thin Films Prepared by RF Magnetron Sputtering of Al Using a N_2/Ar Sputtering Gas Mixture. *Thin Solid Films* **2004**, *469–470*, 184–189.
51. Çakar, M.; Yldrm, N.; Doğan, H.; Türüt, A. The Conductance and Capacitance–Frequency Characteristics of Au/Pyronine-B/P-Type Si/Al Contacts. *Appl. Surf. Sci.* **2007**, *253*, 3464–3468.
52. Papathanassiou, A. N.; Sakellis, I.; Grammatikakis, J. Universal Frequency-Dependent AC Conductivity of Conducting Polymer Networks. *Appl. Phys. Lett.* **2007**, *91*, 122911.
53. Lenski, D. R.; Southard, A.; Fuhrer, M. S. Frequency-Dependent Complex Conductivity of an Organic Thin-Film Transistor. *Appl. Phys. Lett.* **2009**, *94*, 232103.
54. Padma, R.; Lakshmi, B. P.; Reddy, V. R. Capacitance–Frequency (C–F) and Conductance–Frequency (G–F) Characteristics of Ir/N-Ingan Schottky Diode as a Function of Temperature. *Superlattices Microstruct.* **2013**, *60*, 358–369.
55. Gray, H. B.; Winkler, J. R. Long-Range Electron Transfer. *Proc. Natl. Acad. Sci. U.S.A.* **2005**, *102*, 3534–3539.
56. Dyre, J. C.; Schroder, T. B. Universality of AC Conduction in Disordered Solids. *Rev. Mod. Phys.* **2000**, *72*, 873–892.
57. Bradford, M. M. A Rapid and Sensitive Method for the Quantitation of Microgram Quantities of Protein Utilizing the Principle of Protein-Dye Binding. *Anal. Biochem.* **1976**, *72*, 248–254.
58. Kim, K. S.; Zhao, Y.; Jang, H.; Lee, S. Y.; Kim, J. M.; Ahn, J. H.; Kim, P.; Choi, J. Y.; Hong, B. H. Large-Scale Pattern Growth of Graphene Films for Stretchable Transparent Electrodes. *Nature* **2009**, *457*, 706–710.
59. Bae, S.; Kim, H.; Lee, Y.; Xu, X.; Park, J. S.; Zheng, Y.; Balakrishnan, J.; Lei, T.; Kim, H. R.; Song, Y. I.; *et al*. Roll-to-Roll Production of 30-Inch Graphene Films for Transparent Electrodes. *Nat. Nanotechnol.* **2010**, *5*, 574–578.